Measurement of the $\chi_b(3P)$ mass and of the relative rate of $\chi_{b1}(1P)$ and $\chi_{b2}(1P)$ production

LHCb Collaboration ; Bernet, R ; Müller, K ; Steinkamp, O ; Straumann, U ; Vollhardt, A ; et al

Abstract: The production of χ_b mesons in proton-proton collisions is studied using a data sample collected by the LHCb detector, at centre-of-mass energies of $\sqrt{s} = 7$ and 8 TeV and corresponding to an integrated luminosity of 3.0 fb^{-1}. The χ_b mesons are identified through their decays to $\Upsilon(1S)\gamma$ and $\Upsilon(2S)\gamma$ using photons that converted to e^+e^- pairs in the detector. The relative prompt production rate of $\chi_{b1}(1P)$ and $\chi_{b2}(1P)$ mesons is measured as a function of the $\Upsilon(1S)$ transverse momentum in the χ_b rapidity range $2.0 < y < 4.5$. A precise measurement of the $\chi_b(3P)$ mass is also performed. Assuming a mass splitting between the $\chi_{b1}(3P)$ and the $\chi_{b2}(3P)$ states of 10.5 MeV/c^2, the measured mass of the $\chi_{b1}(3P)$ meson is $m(\chi_{b1}(3P)) = 10515.7^{+2.2}_{-3.9}(stat)^{+1.5}_{-2.1}(syst)MeV/c^2$.

DOI: https://doi.org/10.1007/JHEP10(2014)088

Published for SISSA by Springer

Received: *September 5, 2014*
Accepted: *October 1, 2014*
Published: *October 14, 2014*

Measurement of the $\chi_b(3P)$ mass and of the relative rate of $\chi_{b1}(1P)$ and $\chi_{b2}(1P)$ production

The LHCb collaboration

E-mail: tournefier@lapp.in2p3.fr

Abstract: The production of χ_b mesons in proton-proton collisions is studied using a data sample collected by the LHCb detector, at centre-of-mass energies of $\sqrt{s} = 7$ and 8 TeV and corresponding to an integrated luminosity of $3.0\,\text{fb}^{-1}$. The χ_b mesons are identified through their decays to $\Upsilon(1S)\gamma$ and $\Upsilon(2S)\gamma$ using photons that converted to e^+e^- pairs in the detector. The relative prompt production rate of $\chi_{b1}(1P)$ and $\chi_{b2}(1P)$ mesons is measured as a function of the $\Upsilon(1S)$ transverse momentum in the χ_b rapidity range $2.0 < y < 4.5$. A precise measurement of the $\chi_b(3P)$ mass is also performed. Assuming a mass splitting between the $\chi_{b1}(3P)$ and the $\chi_{b2}(3P)$ states of $10.5\,\text{MeV/c}^2$, the measured mass of the $\chi_{b1}(3P)$ meson is

$$m(\chi_{b1}(3P)) = 10515.7^{+2.2}_{-3.9}(\text{stat})^{+1.5}_{-2.1}(\text{syst})\,\text{MeV/c}^2.$$

Keywords: Quarkonium, Hadron-Hadron Scattering, Flavor physics

ArXiv ePrint: 1409.1408

doi:10.1007/JHEP10(2014)088

JHEP10(2014)088

Contents

JHEP10(2014)088

1 Introduction

The study of production and properties of heavy quark-antiquark bound states (quarkonia) provides an important test of the underlying mechanisms described by quantum chromodynamics (QCD). The quarkonium ($c\bar{c}$ and $b\bar{b}$) states in which quarks have parallel spins include the S-wave (J/ψ, Υ) and the P-wave (χ_c, χ_b) states, where each of the latter comprises a closely spaced triplet of $J = 0, 1, 2$ spin states (χ_{cJ}, χ_{bJ}). In high-energy proton-proton collisions at the LHC, $q\bar{q}$ pairs ($q = c, b$) are expected to be produced predominantly via a hard gluon-gluon interaction followed by the formation of bound quarkonium states. The production of the $q\bar{q}$ pair is described by perturbative QCD, while non-perturbative QCD is needed for the description of the evolution of the $q\bar{q}$ pair to the bound state. Several models have been developed for this non-perturbative part such as the colour singlet model [1–3] and the non-relativistic QCD (NRQCD) model [4, 5], which also includes the production of quarkonium via the colour octet mechanism. Recent studies support the leading role of the colour singlet mechanism [6, 7]. Measurements of the relative rate of $J = 1$ and $J = 2$ states provide information on the colour octet contribution. This relative rate is also predicted to have the same dependence on the meson transverse momentum ($p_{\rm T}$) in χ_b and χ_c states, once the $p_{\rm T}$ of the χ_b meson is scaled by the ratio of χ_c and χ_b masses [8].

Measurements of χ_c production and the ratio of the χ_{c1} and χ_{c2} production cross-sections have been made previously using various particle beams and energies [9–13]. All the χ_b states are below the $B\overline{B}$ threshold (where B stands for b mesons) and therefore can be studied through their radiative decays to the Υ mesons, in the same way as the χ_c states were studied through their radiative decays to the J/ψ meson [13].

In this paper we report a measurement of the ratio of $\chi_{b2}(1P)$ to $\chi_{b1}(1P)$ production cross-sections $\sigma(pp \to \chi_{b2}(1P)X)/\sigma(pp \to \chi_{b1}(1P)X)$ at centre-of-mass energies of $\sqrt{s} = 7$ and 8 TeV in the rapidity range $2.0 < y < 4.5$ as a function of the $\Upsilon(1S)$ transverse momentum from 5 to 25 GeV/c. The full LHCb sample is used, corresponding to an integrated luminosity of $3.0\,\text{fb}^{-1}$. The observation in LHCb data of the recently observed $\chi_b(3P)$ state [14, 15] is also presented. The measurement of its mass and of the mass splitting between the $\chi_{bJ}(1P)$ states ($J = 1$ and $J = 2$) provide useful information for testing QCD models [16–18].

The kinematically allowed transitions $\chi_b(1P) \to \Upsilon(1S)\gamma$, $\chi_b(2P) \to \Upsilon(1S)\gamma$, $\chi_b(3P) \to \Upsilon(1S)\gamma$ and $\chi_b(3P) \to \Upsilon(2S)\gamma$ are studied. The $\Upsilon(mS)$ ($m = 1, 2$) meson is reconstructed in the dimuon final state and only photons that convert in the detector material are used. The converted photons are reconstructed using e^+ and e^- tracks, allowing a separation of the χ_{b1} and χ_{b2} mass peaks, due to the improved energy resolution of converted photons with respect to that of photons identified with the calorimeter. Any contribution from the χ_{b0} mesons decays is neglected, as their radiative decay rate is expected to be suppressed by an order of magnitude compared to that of the χ_{b2} meson [17, 19].

2 Detector and data samples

The LHCb detector [20] is a single-arm forward spectrometer covering the pseudorapidity range $2 < \eta < 5$, designed for the study of particles containing b or c quarks. The detector includes a high-precision tracking system consisting of a silicon-strip vertex detector (VELO) surrounding the pp interaction region, a large-area silicon-strip detector station located upstream of a dipole magnet with a bending power of about 4 Tm, and three stations of silicon-strip detectors and straw drift tubes placed downstream of the magnet. The tracking system provides a measurement of momentum, p, with a relative uncertainty that varies from 0.4% at low momentum to 0.6% at 100 GeV/c. The total material before the first tracking station corresponds to about 25% of a radiation length. The minimum distance of a track to a primary vertex, the impact parameter, is measured with a resolution of $(15 + 29/p_{\text{T}})\,\mu\text{m}$, where p_{T} is in GeV/c. Different types of charged hadrons are distinguished using information from two ring-imaging Cherenkov detectors. Photon, electron and hadron candidates are identified by a calorimeter system consisting of scintillating-pad and preshower detectors, an electromagnetic calorimeter (ECAL) and a hadronic calorimeter. The reconstruction of converted photons is described in section 3. Muons are identified by a system composed of alternating layers of iron and multiwire proportional chambers.

The LHCb coordinate system is right-handed with its origin at the nominal interaction point, the z axis aligned along the beam line towards the magnet and the y axis pointing upwards. The magnetic field is oriented along the y axis.

JHEP10(2014)088

The trigger consists of a hardware stage, based on information from the calorimeter and muon systems, followed by a software stage, which applies a full event reconstruction. Events used in this analysis are first required to pass a hardware trigger that selects muon candidates with $p_{\rm T} > 1.76\,{\rm GeV}/c$ or dimuon candidates with a product of their $p_{\rm T}$ larger than $(1.6\,{\rm GeV}/c)^2$. In the software trigger both muons are required to have $p_{\rm T} > 0.5\,{\rm GeV}/c$, total momentum $p > 6\,{\rm GeV}/c$, and dimuon invariant mass greater than $4.7\,{\rm GeV}/c^2$.

In the simulation, pp collisions are generated using Pythia [21, 22] with a specific LHCb configuration [23]. Decays of hadronic particles are described by EvtGen [24], in which final state radiation is generated using Photos [25]. The interaction of the generated particles with the detector and its response are implemented using the Geant4 toolkit [26, 27] as described in ref. [28]. The simulated samples consist of events containing at least one Υ meson that is forced to decay to two muons. In a sample used for background studies, no restriction on the Υ meson production mechanism is imposed. This sample is referred to as *inclusive* Υ in the following. In another sample, used for the estimation of signal efficiencies and parametrisation, the Υ is required to originate from a χ_b meson. This simulated sample is about 10 times larger than the data sample.

3 Event reconstruction and selection

The reconstruction and selection of χ_b candidates closely follows ref. [13]. Photons that convert in the detector material are reconstructed from pairs of oppositely charged electron candidates. Since the acceptance is lower for photons that convert in the VELO and the energy resolution is worse, only $\gamma \to e^+e^-$ candidates without VELO hits are considered. This selection strongly favours conversions that occur between the downstream end of the VELO and the first tracking station upstream of the magnet. The e^+e^- candidates are required to be within the ECAL acceptance and to produce electromagnetic clusters that have compatible coordinates in the non bending plane. Any photon whose position in the ECAL is compatible with a straight line extrapolation of the electron track from the first tracking station is considered as a bremstrahlung photon. Its energy is added to the electron energy. If the same bremsstrahlung candidate is found for both the e^+ and the e^-, the photon energy is added randomly to one of the tracks. The e^+ and e^- tracks (corrected for bremsstrahlung) are then extrapolated backwards in order to determine the conversion point and a vertex fit is performed to reconstruct the photon momentum. The transverse momentum of the photon candidate ($p_{\rm T}^{\gamma}$) is required to be larger than $600\,{\rm MeV}/c$ and the invariant mass of the e^+e^- pair is required to be less than $50\,{\rm MeV}/c^2$, which removes most of the combinatorial background. The resulting purity of the photon sample is determined from simulation to be about 99%.

The Υ candidate is reconstructed in its decay to the $\mu^+\mu^-$ final state. Each track must be identified as a muon with $p_{\rm T} > 2\,{\rm GeV}/c$ and $p > 8\,{\rm GeV}/c$. The two muons must originate from a common vertex with vertex fit χ^2/ndf smaller than 25. Only Υ candidates with transverse momentum ($p_{\rm T}^{\Upsilon}$) greater than 4 GeV/c are kept. Figure 1 shows the invariant mass of Υ candidates. The mass resolution is about 43 MeV/c^2. The accepted mass ranges for the $\Upsilon(1S)$ and for the $\Upsilon(2S)$ candidates are given in table 1.

JHEP10(2014)088

(n,m)	(1,1)	(2,1)	(3,1)	(3,2)
$p_{\mathrm{T}}^{\Upsilon}$ (GeV/c)	> 4.0	> 4.0	> 5.0	> 6.0
p_{T}^{γ} (GeV/c)	> 0.6	> 0.9	> 1.3	> 0.7
Υ mass range (MeV/c^2)	$9360 < m(\mu^+\mu^-) < 9560$			$9960 < m(\mu^+\mu^-) < 10100$
Low mass SB range (MeV/c^2)	$9000 < m(\mu^+\mu^-) < 9200$			$9650 < m(\mu^+\mu^-) < 9850$
High mass SB range (MeV/c^2)	$9650 < m(\mu^+\mu^-) < 9850$			$10150 < m(\mu^+\mu^-) < 10250$

Table 1. Selection criteria for each $\chi_b(nP) \to \Upsilon(mS)\gamma$ transition. SB indicates sideband.

The Υ and γ candidates are each associated with the primary vertex (PV) relative to which they have the smallest impact parameter χ^2, defined as the difference between the χ^2 of the PV reconstructed with and without the considered tracks. They are then combined to form a χ_b candidate. The χ_b decay time has to be smaller than 0.1 ps (about 5 times the observed resolution). Loose requirements are applied in order to reject combinatorial background and poorly reconstructed candidates using the following variables: the difference in z-positions of the primary vertices associated with the Υ and γ candidates, the χ^2 of the χ_b candidate vertex fit and the difference between the χ^2 of the PV fitted with and without the χ_b candidate. These requirements remove about 30% of the background and 8% of the signal. The cosine of the angle between the photon momentum in the χ_b rest frame and the χ_b momentum is required to be positive. This requirement halves the background while preserving 92% of the signal. The χ_b candidates are selected in the rapidity range $2.0 < y < 4.5$.

The χ_b candidates' mass is defined as $m^*(\mu^+\mu^-\gamma) \equiv m(\mu^+\mu^-\gamma) - m(\mu^+\mu^-) + m(\Upsilon)$, where $m(\Upsilon(1S)) = 9460.3 \pm 0.3$ MeV/c^2 and $m(\Upsilon(2S)) = 10023.3 \pm 0.3$ MeV/c^2 are the known Υ mass values [19]. This allows a nearly exact cancellation of the uncertainty due to the Υ mass resolution and any possible bias on the Υ candidates mass. The χ_b mass resolution is therefore dominated by the resolution on the photon energy. The requirements on $p_{\mathrm{T}}^{\Upsilon}$ and p_{T}^{γ} and the Υ signal mass ranges used for each $\chi_b(nP) \to \Upsilon(mS)\gamma$ decay mode are given in table 1.

4 Sample composition and fit model

Two background sources are considered in the sample of χ_b candidates. One source is the non-Υ background originating mainly from the Drell-Yan process where the dimuon pair is combined with a photon. The second source is the combinatorial background where a genuine Υ is combined with a random photon. The functions used for the fits are the sums of a background and signal functions.

The χ_{b1} and χ_{b2} peaks are each parametrised with a double sided Crystal Ball (CB) function [29]:

$$\mathrm{CB}_i(m^*) \propto \exp\left(-\frac{1}{2}\left(\frac{m^* - m_i}{\sigma_i}\right)^2\right) \qquad \text{if} \quad -\alpha_{\mathrm{L}} < \frac{m^* - m_i}{\sigma_i} < \alpha_{\mathrm{R}}$$

JHEP10(2014)088

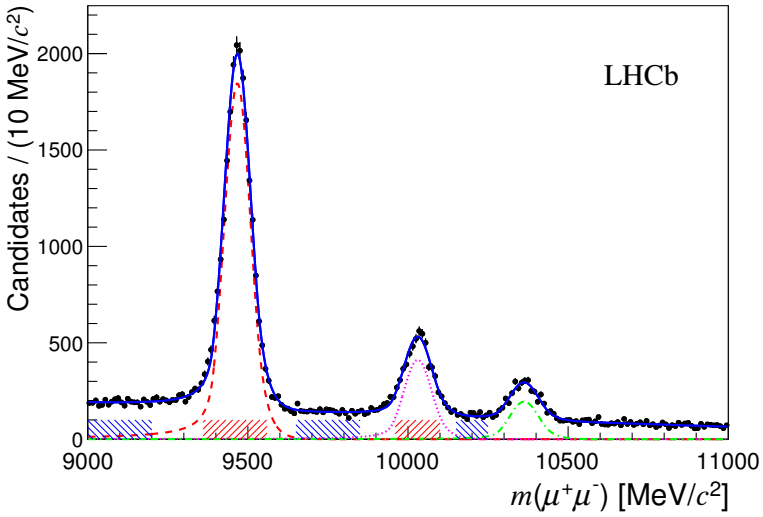

Figure 1. Invariant dimuon mass of the Υ candidates after the event selection requirements and before the Υ mass range requirement. The distribution is fitted with the sum (blue line) of a double-sided Crystal Ball function for each Υ state (dashed red line for $\Upsilon(1S)$, dotted pink line for $\Upsilon(2S)$, dash-dotted green line for $\Upsilon(3S)$) and a second-order polynomial for the background (not shown). The hatched red bands show the signal regions and the hatched blue bands show the mass sidebands used for background studies.

$$\mathrm{CB}_i(m^*) \propto \frac{(n_\mathrm{L}/\alpha_\mathrm{L})^{n_\mathrm{L}}\exp(-\frac{1}{2}\alpha_L^2)}{(n_\mathrm{L}/\alpha_\mathrm{L} - \alpha_\mathrm{L} - (m^* - m_i)/\sigma_i)^{n_\mathrm{L}}} \qquad \text{if} \quad \frac{m^* - m_i}{\sigma_i} < -\alpha_\mathrm{L} \tag{4.1}$$

$$\mathrm{CB}_i(m^*) \propto \frac{(n_\mathrm{R}/\alpha_\mathrm{R})^{n_\mathrm{R}}\exp(-\frac{1}{2}\alpha_\mathrm{R}^2)}{(n_\mathrm{R}/\alpha_\mathrm{R} - \alpha_\mathrm{R} + (m^* - m_i)/\sigma_i)^{n_\mathrm{R}}} \qquad \text{if} \quad \frac{m^* - m_i}{\sigma_i} > \alpha_\mathrm{R},$$

where the index $i = 1(2)$ refers to the χ_{b1} (χ_{b2}) CB function. The CB left tail accounts for events with unreconstructed bremsstrahlung, while the right tail accounts for events with overcorrected bremsstrahlung. Simulation shows that the same tail parameters α_R and $n_\mathrm{L,R}$ can be used for all the $\chi_{bi}(nP)$ states, $n_\mathrm{L} = n_\mathrm{R} = 2.5$ and $\alpha_\mathrm{R} = 1.0$, while different values of α_L have to be used: $\alpha_\mathrm{L} = 0.20$, 0.25 and 0.30, for the $\chi_{bi}(1P)$, $\chi_{bi}(2P)$ and $\chi_{bi}(3P)$ shapes, respectively. Since in the study of χ_c states it was found that the CB tail parameters were similar in data and simulation [13], the values found with simulation are used for the χ_b. The CB width, σ, increases with the mass difference between the considered χ_b and Υ states. Fits to the mass distributions of $\chi_b(1P) \to \Upsilon(1S)\gamma$ and $\chi_b(2P) \to \Upsilon(1S)\gamma$ candidates indicate that the width is $10\% - 20\%$ larger in data than in simulation. Therefore, the CB width is fixed to the value found with simulated events increased by 10% and it is varied by $\pm 10\%$ for studies of the systematic effects.

The shape of the non-Υ background and its amplitude are estimated using the Υ mass sidebands shown in figure 1 and given in table 1. The mass distribution of these candidates is fitted with an empirical function

$$f_\mathrm{bkg}(m^*) \propto \arctan\left(\frac{m^* - m_0}{c}\right) + b\left(\frac{m^*}{m_0} - 1\right) + a\,, \tag{4.2}$$

JHEP10(2014)088

where m_0, a, b and c are free parameters. This function is then used to parametrise the non-Υ background contribution with all parameters fixed to the fitted values. The shape of the combinatorial background is estimated using the inclusive Υ simulated sample and parametrised with eq. (4.2). All parameters are fixed to the values found with simulation except for the normalisation. In the case of the $\chi_b(3P) \to \Upsilon(2S)\gamma$ transition, this shape does not reproduce the data properly and the value of the m_0 parameter is therefore left free in the fit. This discrepancy is due to mismodeling of the $p_{\mathrm{T}}^{\Upsilon}$ spectrum in simulation and is accounted for in the systematic uncertainties.

The fits have at most six free parameters: the mean mass value for the χ_{b1} peak m_1, the mass difference between the χ_{b2} and χ_{b1} peaks Δm_{12}, the normalisation of the χ_{b1} CB function A_1, the ratio of the χ_{b2} to χ_{b1} CB amplitudes r_{12}, the normalisation of the combinatorial background A_{comb} and the m_0 parameter for the combinatorial background shape.

5 χ_b meson masses

5.1 Mass measurements

The masses of the χ_b mesons are determined using unbinned maximum likelihood fits to the χ_b mass distributions using the parametrisation described in section 4. Figures 2 (a) and (b) show the mass distributions for the $\chi_b(1P) \to \Upsilon(1S)\gamma$ and $\chi_b(2P) \to \Upsilon(1S)\gamma$ decays with the fit results overlaid. In these fits the free parameters are m_1, A_1, Δm_{12}, r_{12} and A_{comb}. Table 2 reports the resulting mass determinations for these states compared to the world average values [19]. A small bias is expected on the measured masses, attributed to unreconstructed bremsstrahlung of the e^+e^- pair. This bias is proportional to the Q-value of the transition and is expected, from simulation, to be about -0.5 and -1.5 MeV/c^2 for the $\chi_b(1P) \to \Upsilon(1S)\gamma$ and $\chi_b(2P) \to \Upsilon(1S)\gamma$ decays, respectively. The measurements given in table 2 are not corrected for this bias and are consistent with such a bias. On the other hand the $\chi_b(3P)$ mass measured using the $\chi_b(3P) \to \Upsilon(mS)\gamma$ transitions is corrected for the bias estimated with simulation, $-3.0 \pm 2.0\,\mathrm{MeV}/c^2$ and -0.5 ± 0.5 MeV/c^2 for $m = 1$ and $m = 2$, respectively, where the uncertainties cover possible discrepancies between data and simulation.

In the case of the $\chi_b(3P)$ meson, the mass splitting and the relative yields are also fixed, as the spin-1 and spin-2 peaks cannot be separated. Theory predictions vary from 9 to 12 MeV/c^2 [16, 17] for Δm_{12} and this parameter is fixed to 10.5 MeV/c^2. The value of r_{12} is fixed based on theoretical predictions [17] and our experimental measurement. It can be expressed as the product of the ratio of branching fractions to $\Upsilon\gamma$ and of the ratio of production cross-sections of the $\chi_{b2}(3P)$ and $\chi_{b1}(3P)$ states. Predictions for branching fractions are found in refs. [17, 18]. The predictions from ref. [17] agree well with the experimental measurements for the $\chi_b(1P)$ and the $\chi_b(2P)$ mesons. The model of ref. [17] predicts similar values for the two transitions, $\mathcal{B}(\chi_{b2}(3P) \to \Upsilon(mS)\gamma))/\mathcal{B}(\chi_{b1}(3P) \to \Upsilon(mS)\gamma) \approx 0.47$ $(m = 1, 2)$. According to ref. [8] the ratio of production cross-sections is expected to be the same for the $\chi_b(3P)$ and $\chi_b(1P)$ mesons and thus, using the measurement detailed in section 6, we obtain $\sigma(\chi_{b2}(nP))/\sigma(\chi_{b1}(nP)) = 0.9 \pm 0.2$.

JHEP10(2014)088

(n,m)	(1,1)	(2,1)
m_1	9892.3 ± 0.5	10254.7 ± 1.3
m_1 world average	9892.8 ± 0.4	10255.5 ± 0.6
Δm_{12}	19.81 ± 0.65	12.3 ± 2.6
Δm_{12} world average	19.43 ± 0.37	13.5 ± 0.6

Table 2. Fitted values of the $\chi_b(nP)$ $(n = 1, 2)$ masses (in MeV/c^2) from the $\chi_b(nP) \to \Upsilon(1S)\gamma$ transitions, compared to the world average values. The uncertainties are statistical only.

(n,m)	(3,1)	(3,2)	(3,1)+(3,2)
m_1	$10509.0^{+5.0}_{-2.6}$	$10518.5^{+1.9}_{-1.3}$	$10515.7^{+2.2}_{-3.9}$
Δm_{12}	10.5 (fixed)	10.5 (fixed)	10.5 (fixed)
$N(\chi_b)$	107 ± 19	41 ± 12	169 ± 25

Table 3. Fitted values of the $\chi_b(3P)$ mass (in MeV/c^2) for the $\chi_b(3P) \to \Upsilon(mS)\gamma$ $(m = 1, 2)$ transitions. The last column gives the result of the simultaneous fit to the two transitions. The values are corrected for the mass bias (-3 MeV/c^2 and -0.5 MeV/c^2 for the $\Upsilon(1S)$ and $\Upsilon(2S)$ transitions, respectively). The last row gives the total χ_b yields. The uncertainties are statistical only.

To summarise, the value $r_{12} = 0.47 \times 0.9 = 0.42$ is used in the fits to the mass distributions associated with the transitions of the $\chi_b(3P)$ meson to $\Upsilon(1S)$ and $\Upsilon(2S)$ mesons. Table 3 gives the result of the fits to the mass distributions for the $\chi_b(3P) \to \Upsilon(1S)\gamma$ and $\chi_b(3P) \to \Upsilon(2S)\gamma$ transitions. A simultaneous fit to these two distributions is also performed and the result is reported in the last column of table 3. Figure 2 shows the results of these fits. The $\chi_b(3P) \to \Upsilon(1S)\gamma$ and $\chi_b(3P) \to \Upsilon(2S)\gamma$ decays are seen with a statistical significance, determined from the likelihood ratio of the fits with background only and with signal plus background hypotheses, of 6.0σ and 3.6σ respectively. The total statistical significance determined with the simultaneous fit is 6.9σ.

5.2 Systematic uncertainties

The systematic uncertainties on the measurement of the $\chi_b(nP)$ $(n = 1, 2)$ mass splitting and of the $\chi_b(3P)$ mass are detailed as follows.

First the systematic uncertainties related to the signal parametrisation are considered. The χ_{b0} contribution is expected to be small because its branching fraction to $\Upsilon(1S)\gamma$ is less than 2% for $\chi_b(1P)$ and $\chi_b(2P)$ mesons [19]. In order to estimate the systematic uncertainty due to the presence of a χ_{b0} or another unknown state, a third CB function is added to the fit, with a peak position fixed to the world average value for the $\chi_b(nP)$ for $n = 1, 2$ and left free for the $\chi_b(3P)$. The resulting yield of χ_{b0} mesons is compatible with zero. The Gaussian width of the CB function is varied within $\pm 10\%$ to cover possible differences between data and simulation. For these two fit variations, the differences between results of the nominal and alternative fits are taken as systematic uncertainties, added in quadrature and referred to as *signal* uncertainty in table 4.

JHEP10(2014)088

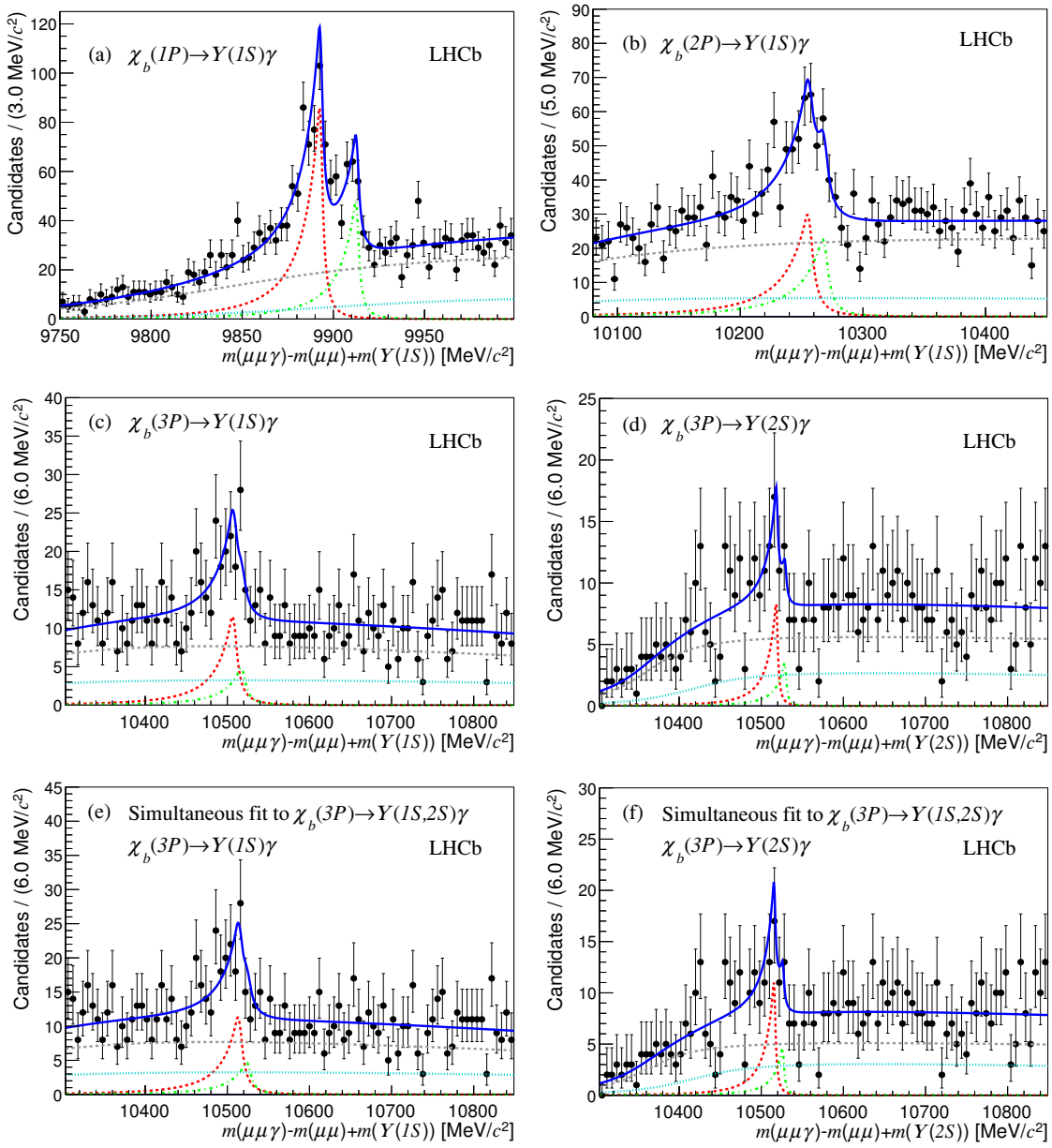

Figure 2. Distribution of $m^*(\mu^+\mu^-\gamma) \equiv m(\mu^+\mu^-\gamma) - m(\mu^+\mu^-) + m(\Upsilon)$ for χ_b candidates with fit projections overlaid for (a) $\chi_b(1P) \to \Upsilon(1S)\gamma$, (b) $\chi_b(2P) \to \Upsilon(1S)\gamma$, (c,e) $\chi_b(3P) \to \Upsilon(1S)\gamma$ and (d,f) $\chi_b(3P) \to \Upsilon(2S)\gamma$ channels. The result of the simultaneous fit to the $\chi_b(3P) \to \Upsilon(1S)\gamma$ and $\chi_b(3P) \to \Upsilon(2S)\gamma$ mass distributions is shown in (e) and (f). The cyan dotted line shows the non-Υ background, the grey dashed line shows the combinatorial background, the red dashed line the χ_{b1} contribution, the green dash-dotted line the χ_{b2} contribution, and the blue full line the sum of all these contributions.

JHEP10(2014)088

Imperfect modelling of the background is also considered as a possible source of systematic uncertainty. The normalisation of the non-Υ background is varied within the uncertainty of the estimated number of background events under the Υ peak (typically 10%). Negligible variations are observed when the shape of this background is determined using only the low or the high mass sideband. Therefore no systematic uncertainty is assigned from the non-Υ background modelling. The shape of the combinatorial background is particularly sensitive to the m_0 value, therefore this parameter is varied within twice its uncertainty. In the case of the $\chi_b(3P) \to \Upsilon(2S)\gamma$ transition, where the value of m_0 is left free in the fit, the value found in simulation is used in an alternative fit, leading to a change of 0.1 MeV/c^2 on the $\chi_b(3P)$ mass. The fit range is also varied by ± 100 MeV/c^2 on both sides. The differences between results of the nominal fit and these two alternative fits are taken as systematic uncertainties and added in quadrature. The resulting systematic uncertainty is referred to as *background* uncertainty.

The uncertainty on the mass bias (2.0 and 0.5 MeV/c^2 for the $\chi_b(3P)$ mass measurement based on the transition to $\Upsilon(1S)$ and $\Upsilon(2S)$ respectively) is assigned as systematic uncertainty. For the simultaneous fit to the two $\chi_b(3P)$ mass distributions, the two biases are varied independently within their uncertainties and the largest variation is taken as systematic uncertainty. A small bias is expected on the $\chi_b(1P)$ mass splitting and is estimated to be at most 0.10 MeV/c^2, which is added as a systematic uncertainty. No significant bias on the $\chi_b(nP)$ mass splitting is expected from the fit procedure.

For the determination of the $\chi_b(3P)$ mass, the Δm_{12} and r_{12} parameters are fixed in the nominal fit. They are varied independently within their expected uncertainties in order to evaluate the associated systematic uncertainties. The mass splitting, Δm_{12}, is varied between 9 and 12 MeV/c^2 and the r_{12} parameter is varied by $\pm 30\%$, which includes theoretical uncertainties and the precision on the $\chi_b(1P)$ production ratio measured in this work and used to estimate r_{12}.

Finally, the 0.3 MeV/c^2 uncertainty on the world-average values of the $\Upsilon(1S)$ and $\Upsilon(2S)$ masses is added as a systematic uncertainty to the $\chi_b(3P)$ mass.

Table 4 lists the individual systematic uncertainties. The total systematic uncertainty is the quadratic sum of all individual uncertainties.

6 Relative rate of $\chi_{b2}(1P)$ and $\chi_{b1}(1P)$ production

6.1 Measurement of the relative rates

The production cross-section ratio of the $\chi_{b2}(1P)$ and $\chi_{b1}(1P)$ mesons is measured in three $p_{\rm T}^{\Upsilon}$ ranges of different size (the bin limits are given in table 5) using

$$\frac{\sigma(\chi_{b2})}{\sigma(\chi_{b1})} = \frac{N_{\chi_{b2}}}{N_{\chi_{b1}}} \frac{\varepsilon_{\chi_{b1}}}{\varepsilon_{\chi_{b2}}} \frac{\mathcal{B}(\chi_{b1} \to \Upsilon(1S)\gamma)}{\mathcal{B}(\chi_{b2} \to \Upsilon(1S)\gamma)}, \tag{6.1}$$

where $\sigma(\chi_{bJ})$ $(J = 1, 2)$ is the $\chi_{bJ}(1P)$ meson production cross-section; $N_{\chi_{bJ}}$ is the $\chi_{bJ}(1P)$ yield; $\varepsilon_{\chi_{bJ}}$ is the efficiency to trigger, detect, reconstruct and select a χ_{bJ} meson including the contribution from the approximately 20% probability for a photon to convert upstream

JHEP10(2014)088

	Δm_{12}(1P)	Δm_{12}(2P)	$m(\chi_{b1}(3P))$ from $\Upsilon(1S)$	$m(\chi_{b1}(3P))$ from $\Upsilon(2S)$	$m(\chi_{b1}(3P))$ combined
Signal	±0.16	±0.5	±0.3	±0.1	±0.6
Background	±0.08	±0.3	±0.2	±0.1	±0.2
Bias	±0.10	±0.1	±2.0	±0.5	$^{+1.2}_{-1.6}$
r_{12}	-	-	$^{+0.7}_{-0.4}$	$^{+0.1}_{-0.2}$	$^{+0.6}_{-1.1}$
Δm_{12}	-	-	±1.2	±0.1	±0.3
$m(\Upsilon)$	-	-	±0.3	±0.3	±0.3
Total	±0.20	±0.6	$^{+2.5}_{-2.4}$	±0.6	$^{+1.5}_{-2.1}$

Table 4. Summary of the systematic uncertainties on the $\chi_b(nP)$ $(n = 1, 2)$ mass splitting and on the $\chi_{b1}(3P)$ mass in MeV/c^2. The last column refers to the simultaneous fit to the two transitions.

$p_{\rm T}^{\Upsilon}$ bin (GeV/c)	5–10	10–15	15–25
$N(\chi_{b2})/N(\chi_{b1})$	0.61 ± 0.15	0.57 ± 0.15	0.52 ± 0.15
$\varepsilon(\chi_{b1})/\varepsilon(\chi_{b2})$	1.01 ± 0.03	0.90 ± 0.05	1.18 ± 0.11

Table 5. Relative rate of $\chi_{b1}(1P)$ and $\chi_{b2}(1P)$ production and ratio of total efficiency (in the three $p_{\rm T}^{\Upsilon}$ ranges). Uncertainties only refer to the statistical contributions.

of the first tracking station; and $\mathcal{B}(\chi_{b1}(1P) \to \Upsilon(1S)\gamma) = (33.9 \pm 2.2)\%$ and $\mathcal{B}(\chi_{b2}(1P) \to \Upsilon(1S)\gamma) = (19.1 \pm 1.2)\%$ are the known branching fractions [19] .

The inefficiency is dominated by the converted photon acceptance and reconstruction: low-energy photons produce low-energy electrons, which have a high chance to escape the detector due to the magnetic field. The efficiency of converted photon reconstruction and selection relative to non-converted photons is measured in ref. [13] and ranges from about 1% at $p_{\rm T}^{\gamma}$ of 600 MeV/c to 3% at $p_{\rm T}^{\gamma}$ of 2000 MeV/c. These numbers include the conversion probability. Due to the correlation between the $p_{\rm T}$ of the photon and that of the Υ meson, the efficiency is lower for low $p_{\rm T}^{\Upsilon}$. The ratio of efficiencies is given in table 5. This ratio differs from unity because the $p_{\rm T}^{\Upsilon}$ spectrum is different for χ_{b1} and χ_{b2} in Pythia 8, as expected [8]. The ratio of efficiencies is also calculated assuming equal $p_{\rm T}$ spectra. It is still slightly different from unity due to the small difference in the χ_{b1} and χ_{b2} masses.

The mass distribution of χ_b candidates in each $p_{\rm T}^{\Upsilon}$ bin is fitted using the signal and background functions described in section 4. In these fits the mass of the χ_{b1} state and the mass splitting are fixed to the values found from the fit to the whole data set (see table 2) and then varied within their uncertainties for systematic studies. The result of the fit is shown in figure 3 and the ratio of yields is given in table 5 for each $p_{\rm T}^{\Upsilon}$ range.

6.2 Systematic uncertainties

The same sources of systematic uncertainties as for the mass measurements (see section 5.2) are investigated and reported in table 6. Additional systematic checks relevant only for the relative rates of $\chi_{b2}(1P)$ and $\chi_{b1}(1P)$ are detailed as follows.

JHEP10(2014)088

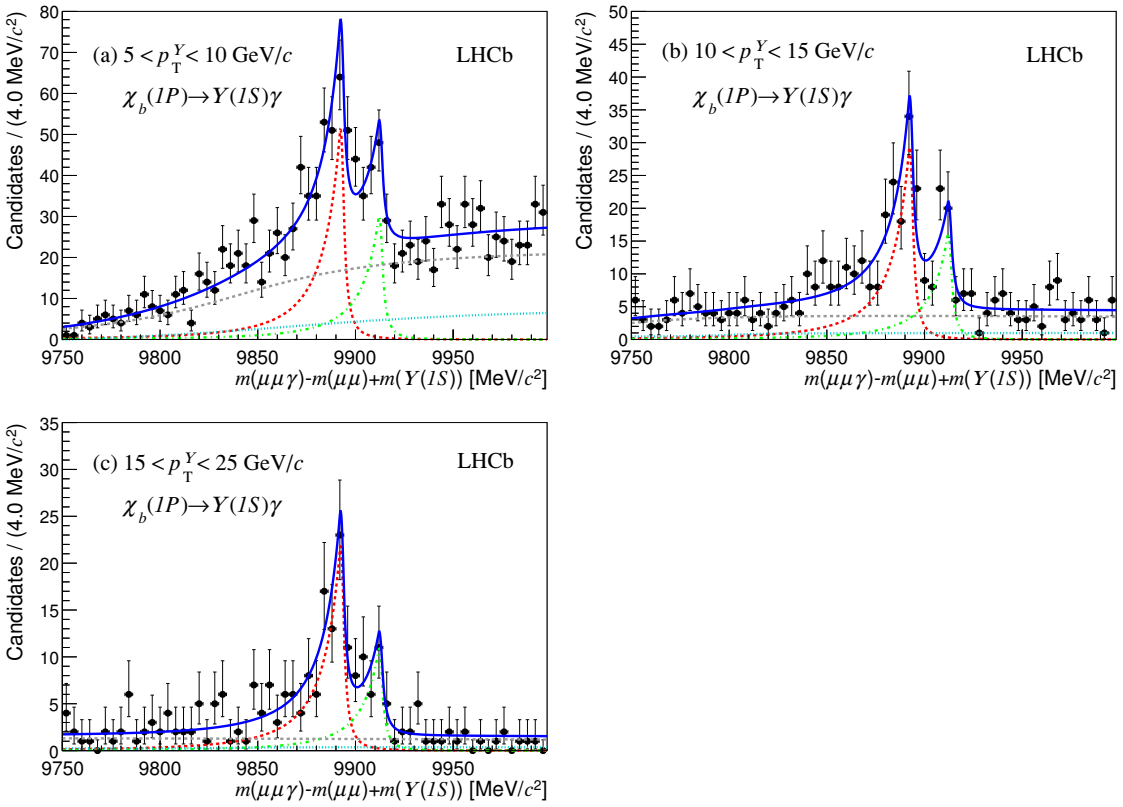

Figure 3. Distribution of $m^*(\mu^+\mu^-\gamma) \equiv m(\mu^+\mu^-\gamma) - m(\mu^+\mu^-) + m(\Upsilon)$ for $\chi_b(1P)$ candidates with fit projections overlaid for each of the three ranges in p_T^Υ: (a) 5–10 GeV/c, (b) 10–15 GeV/c and (c) 15–25 GeV/c. The cyan dotted line show the non-Υ background, the grey dashed line shows the combinatorial background, the red dashed line the χ_{b1} contribution, the green dash-dotted line the χ_{b2} contribution and the blue full line the sum of all these contributions.

The dominant uncertainty on the ratio of efficiencies is due to the limited knowledge of the efficiency for reconstructing converted photons, which is estimated following ref. [13] and amounts to 4% on the relative rates. This uncertainty is added in quadrature to the uncertainty due to the limited size of the simulated sample.

Due to the large size of the p_T bins, the efficiency depends on the choice of the p_T spectrum of χ_b production as discussed in section 6.1. In order to assess the uncertainty due to the shape of the p_T spectrum, the simulated χ_{b2} (χ_{b1}) spectrum is changed to be identical to the simulated χ_{b1} (χ_{b2}) spectrum. The relative difference in the ratio of efficiencies is taken as a systematic uncertainty.

The fit is also performed on simulated data and a mean bias of $(-4 \pm 4)\%$ is observed on the relative yields. A systematic uncertainty of $\pm 4\%$ is added to take the possible bias into account. The values of the $\chi_{b1}(1P)$ mass m_1 and of the mass splitting Δm_{12} are also varied within their uncertainties from table 2. The variation of the result is taken as systematic uncertainty and is added in quadrature to the uncertainty referred to as *signal*.

JHEP10(2014)088

$p_{\rm T}^{\Upsilon}$ bin (GeV/c)	5–10	10–15	15–25
Signal	±0.05	±0.08	±0.08
Background	±0.06	±0.04	±0.03
Fit bias	±0.04	±0.04	±0.04
Efficiency	±0.05	±0.06	±0.10
$p_{\rm T}$ model	-0.13	-0.05	-0.04
Total	$^{+0.10}_{-0.16}$	$^{+0.12}_{-0.13}$	$^{+0.13}_{-0.14}$

Table 6. Summary of the systematic uncertainties on the $\chi_b(1P)$ relative rates, expressed as fractions of the relative rate.

Table 6 lists the systematic uncertainties on the relative rates. The total systematic uncertainty is the quadratic sum of all individual uncertainties. The ratio of cross-sections is also affected by the uncertainties on the branching fraction of $\chi_b(1P) \to \Upsilon(1S)\gamma$, leading to an additional systematic uncertainty of 9.0% [19].

7 Results

The results for the $\chi_b(1,2P)$ mass splittings between the $J = 1$ and $J = 2$ states

$$\Delta m_{12}(1P) = 19.81 \pm 0.65(\text{stat}) \pm 0.20(\text{syst})\,\text{MeV}/c^2$$
$$\Delta m_{12}(2P) = 12.3 \pm 2.6(\text{stat}) \pm 0.6(\text{syst})\,\text{MeV}/c^2$$

are in agreement with the world average values, $\Delta m_{12}(1P) = 19.43 \pm 0.37\,\text{MeV}/c^2$ and $\Delta m_{12}(2P) = 13.5 \pm 0.6\,\text{MeV}/c^2$ [19]. A measurement of the $\chi_{b1}(3P)$ mass,

$$m(\chi_{b1}(3P)) = 10509.0^{+5.0}_{-2.6}(\text{stat})^{+2.5}_{-2.4}(\text{syst})\,\text{MeV}/c^2,$$

is derived from the radiative transition to the $\Upsilon(1S)$ meson, where the $\chi_b(3P)$ is observed with a statistical significance of 6.0σ. Another measurement,

$$m(\chi_{b1}(3P)) = 10518.5^{+1.9}_{-1.3}(\text{stat}) \pm 0.6(\text{syst})\,\text{MeV}/c^2,$$

is derived from the radiative transition to the $\Upsilon(2S)$ transition, where evidence is found for the $\chi_b(3P)$ with a statistical significance of 3.6σ. The systematic uncertainty related to r_{12} is largely uncorrelated between the $\Upsilon(2S)$ and $\Upsilon(1S)$ channels as the branching fractions of χ_{bi} to final states involving $\Upsilon(1S)$ and to $\Upsilon(2S)$ mesons can be different. By treating the systematic uncertainties related to the mass splitting and to the mass bias as fully correlated and all other uncertainties as uncorrelated, the two results for the $\chi_{b1}(3P)$ mass differ by $9.3^{+3.2}_{-5.2}(\text{stat}) \pm 2.0(\text{syst})$ MeV/c^2. A combined fit is performed leading to

$$m(\chi_{b1}(3P)) = 10515.7^{+2.2}_{-3.9}(\text{stat})^{+1.5}_{-2.1}(\text{syst})\,\text{MeV}/c^2.$$

In these measurements, the relative rate of χ_{b2} to χ_{b1}, is assumed to be $r_{12} = 0.42$ for the two transitions. The $\chi_{b1}(3P)$ mass result exhibits a linear dependence on the assumed

JHEP10(2014)088

$p_{\rm T}^{\Upsilon}$ bin (GeV/c)	$\sigma(\chi_{b2})/\sigma(\chi_{b1})$
5–10	$1.09 \pm 0.27(\text{stat})^{+0.11}_{-0.18}(\text{syst}) \pm 0.10\,(\mathcal{B})$
10–15	$0.91 \pm 0.24(\text{stat})^{+0.10}_{-0.12}(\text{syst}) \pm 0.08\,(\mathcal{B})$
15–25	$1.09 \pm 0.31(\text{stat})^{+0.14}_{-0.15}(\text{syst}) \pm 0.10\,(\mathcal{B})$

Table 7. Relative production cross section of χ_{b1} to χ_{b2} mesons for the $1P$ state for each $p_{\rm T}^{\Upsilon}$ bin. The first uncertainty is statistical, the second is the systematic uncertainty and the third is due to the uncertainty on the branching fractions.

fraction of χ_{b1} decays and varies from 10517.6 to 10515.2 when the χ_{b2}/χ_{b1} yield ratio changes from zero to 0.5. This result is compatible with and significantly more precise than that reported by the ATLAS experiment, $m(\chi_b(3P)) = 10530 \pm 5(\text{stat}) \pm 9(\text{syst})\,\text{MeV}/c^2$ for $r_{12} = 1$ and $\Delta m_{12} = 12\,\text{MeV}/c^2$, where $m(\chi_b(3P))$ is the average mass of χ_{b1} and χ_{b2} states [14]. The LHCb result is also compatible with the D0 measurement, $m(\chi_b(3P)) = 10551 \pm 14(\text{stat}) \pm 17(\text{syst})\,\text{MeV}/c^2$ [15].

The ratio of the χ_{b2} to χ_{b1} production cross-sections is measured in three $p_{\rm T}^{\Upsilon}$ ranges using eq. (6.1). The results are given in table 7. Figure 4 (a) shows a comparison of the measured values with LO NRQCD predictions from ref. [8]. The common systematic uncertainty (9.0%) due to the branching fraction of $\chi_b \to \Upsilon(1S)\gamma$ is not shown. Theory predicts the χ_c and χ_b ratio of production cross-section to be the same when the χ_c $p_{\rm T}$ value is scaled by the ratio of the χ_b and χ_c masses [8]. As the $\chi_b(\chi_c)$ and Υ (J/ψ) $p_{\rm T}$ are strongly correlated, this is assumed to be valid when replacing the $\chi_b(\chi_c)$ by the Υ (J/ψ) $p_{\rm T}$. The measurement obtained by LHCb for the χ_c production ratio [13] with the $p_{\rm T}$ axis scaled accordingly is also shown for comparison. The χ_b results are in good agreement with the scaled χ_c results. These results are not precise enough to establish the deviation from unity predicted by theory at low $p_{\rm T}$, but the agreement is better with a flat dependence. Our results are also in agreement with the CMS results [30] as shown on figure 4 (b).

8 Conclusion

The radiative decays of χ_b mesons to Υ mesons are reconstructed with photons converting in the detector material. Owing to the good energy resolution obtained with converted photons, the $\chi_b(1P)$ states are separated and the mass splitting between the $\chi_{b1}(1P)$ and $\chi_{b2}(1P)$ is measured. The $\chi_b(3P)$ mass is measured using its radiative decays to the $\Upsilon(1S)$ and $\Upsilon(2S)$ mesons yielding,

$$m(\chi_{b1}(3P)) = 10515.7^{+2.2}_{-3.9}(\text{stat})^{+1.5}_{-2.1}(\text{syst})\,\text{MeV}/c^2.$$

This result is compatible with the measurement performed by LHCb with the radiative decays to the $\Upsilon(3S)$ meson that uses non-converted photons [31], $m(\chi_{b1}(3P)) = 10511.3 \pm 1.7(\text{stat}) \pm 2.5(\text{syst})$ MeV/c^2. Since the photon reconstruction is based on different subdetectors, the experimental systematic uncertainties are uncorrelated, while the

JHEP10(2014)088

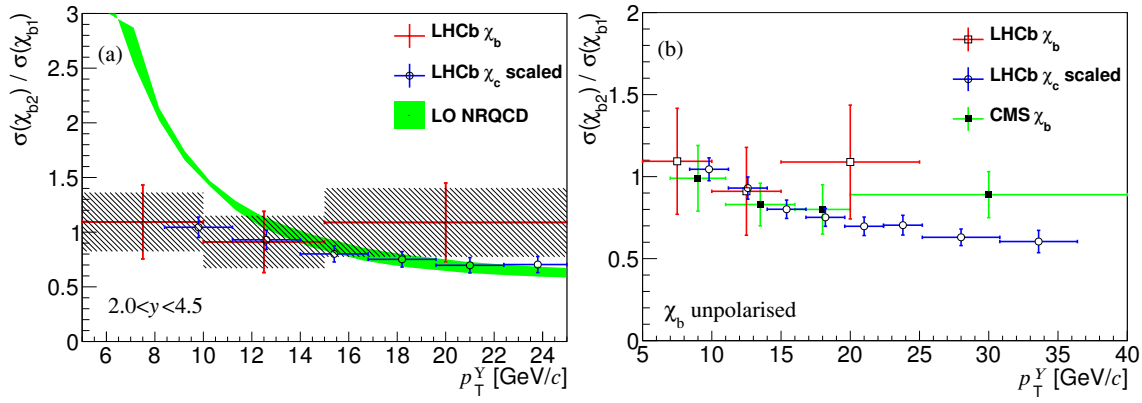

Figure 4. Relative production cross-sections of χ_{b1} to χ_{b2} mesons as a function of $p_{\mathrm{T}}^{\Upsilon}$. Panel (a) shows the comparison of this measurement (the hatched rectangles show the statistical uncertainties and the red crosses the total experimental uncertainty) to the LO NRQCD prediction [8] (green band), and to the LHCb χ_c result (blue crosses), where the p_{T} axis has been scaled by $m(\chi_b)/m(\chi_c) = 2.8$. Panel (b) compares this measurement (empty squares) to CMS results [30] (filled squares) and to the scaled LHCb χ_c results (empty circles). The error bars are the total experimental uncertainties and do not include the uncertainties on the branching fractions.

uncertainty related to the model used for summing the $J = 1$ and $J = 2$ contributions (parametrised with the mass splitting Δm_{12} and the relative rates r_{12}) are fully correlated. The combined value is

$$m(\chi_{b1}(3P)) = 10512.1 \pm 2.1(\mathrm{exp}) \pm 0.9(\mathrm{model})\,\mathrm{MeV}/c^2,$$

where the first uncertainty is experimental (statistical and systematic) and the second accounts for varying Δm_{12} from 9.0 to 12.0 MeV/c^2 and r_{12} by $\pm 30\%$. This result is in agreement with the theoretical prediction of ref. [17], $m(\chi_{b1}(3P)) = 10516$ MeV/c^2.

The first measurement of the relative ratio of χ_{b1} to χ_{b2} cross-sections is performed for the $\chi_b(1P)$ state in the rapidity range $2.0 < y < 4.5$ for $p_{\mathrm{T}}^{\Upsilon}$ from 5 to 25 GeV/c. The results agree with CMS results [30] and with theory expectation based on LHCb χ_c measurements [13]. The data indicate a deviation from the rise predicted by the LO NRQCD model at low p_{T} and show a better agreement with a flat dependence.

Acknowledgments

We thank A. Luchinsky and A. Likhoded for providing the LO NRQCD predictions. We express our gratitude to our colleagues in the CERN accelerator departments for the excellent performance of the LHC. We thank the technical and administrative staff at the LHCb institutes. We acknowledge support from CERN and from the national agencies: CAPES, CNPq, FAPERJ and FINEP (Brazil); NSFC (China); CNRS/IN2P3 (France); BMBF, DFG, HGF and MPG (Germany); SFI (Ireland); INFN (Italy); FOM and NWO (The Netherlands); MNiSW and NCN (Poland); MEN/IFA (Romania); MinES and FANO (Russia); MinECo (Spain); SNSF and SER (Switzerland); NASU (Ukraine); STFC (United

JHEP10(2014)088

Kingdom); NSF (U.S.A.). The Tier1 computing centres are supported by IN2P3 (France), KIT and BMBF (Germany), INFN (Italy), NWO and SURF (The Netherlands), PIC (Spain), GridPP (United Kingdom). We are indebted to the communities behind the multiple open source software packages on which we depend. We are also thankful for the computing resources and the access to software R&D tools provided by Yandex LLC (Russia). Individual groups or members have received support from EPLANET, Marie Skłodowska-Curie Actions and ERC (European Union), Conseil général de Haute-Savoie, Labex ENIGMASS and OCEVU, Région Auvergne (France), RFBR (Russia), XuntaGal and GENCAT (Spain), Royal Society and Royal Commission for the Exhibition of 1851 (United Kingdom).

JHEP10(2014)088

References

[1] R. Baier and R. Ruckl, *Hadronic collisions: a quarkonium factory*, *Z. Phys.* **C 19** (1983) 251 [INSPIRE].

[2] V.G. Kartvelishvili, A.K. Likhoded and S.R. Slabospitsky, *D meson and ψ meson production in hadronic interactions*, *Sov. J. Nucl. Phys.* **28** (1978) 678 [*Yad. Fiz.* **28** (1978) 1315] [INSPIRE].

[3] E.L. Berger and D.L. Jones, *Inelastic photoproduction of J/ψ and Υ by gluons*, *Phys. Rev.* **D 23** (1981) 1521 [INSPIRE].

[4] G.T. Bodwin, E. Braaten and G.P. Lepage, *Rigorous QCD analysis of inclusive annihilation and production of heavy quarkonium*, *Phys. Rev.* **D 51** (1995) 1125 [*Erratum ibid.* **D 55** (1997) 5853] [hep-ph/9407339] [INSPIRE].

[5] Y.-Q. Ma, K. Wang and K.-T. Chao, *QCD radiative corrections to χ_{cJ} production at hadron colliders*, *Phys. Rev.* **D 83** (2011) 111503 [arXiv:1002.3987] [INSPIRE].

[6] J.-P. Lansberg, *On the mechanisms of heavy-quarkonium hadroproduction*, *Eur. Phys. J.* **C 61** (2009) 693 [arXiv:0811.4005] [INSPIRE].

[7] J.M. Campbell, F. Maltoni and F. Tramontano, *QCD corrections to J/ψ and Υ production at hadron colliders*, *Phys. Rev. Lett.* **98** (2007) 252002 [hep-ph/0703113] [INSPIRE].

[8] A.K. Likhoded, A.V. Luchinsky and S.V. Poslavsky, *Production of χ_b-mesons at LHC*, *Phys. Rev.* **D 86** (2012) 074027 [arXiv:1203.4893] [INSPIRE].

[9] WA11 collaboration, Y. Lemoigne et al., *Measurement of hadronic production of the $\chi_1^{++}(3507)$ and the $\chi_2^{++}(3553)$ through their radiative decay to J/ψ*, *Phys. Lett.* **B 113** (1982) 509 [*Erratum ibid.* **B 116** (1982) 470] [INSPIRE].

[10] HERA-B collaboration, I. Abt et al., *Production of the charmonium states χ_{c1} and χ_{c2} in proton nucleus interactions at $\sqrt{s} = 41.6$ GeV*, *Phys. Rev.* **D 79** (2009) 012001 [arXiv:0807.2167] [INSPIRE].

[11] CDF collaboration, A. Abulencia et al., *Measurement of $\sigma_{\chi_{c2}}\mathcal{B}(\chi_{c2} \to J/\psi\gamma)/\sigma_{\chi_{c1}}\mathcal{B}(\chi_{c1} \to J/\psi\gamma)$ in $p\bar{p}$ collisions at $\sqrt{s} = 1.96$ TeV*, *Phys. Rev. Lett.* **98** (2007) 232001 [hep-ex/0703028] [INSPIRE].

[12] CMS collaboration, *Measurement of the relative prompt production rate of χ_{c2} and χ_{c1} in pp collisions at $\sqrt{s} = 7$ TeV*, *Eur. Phys. J.* **C 72** (2012) 2251 [arXiv:1210.0875] [INSPIRE].

[13] LHCb collaboration, *Measurement of the relative rate of prompt χ_{c0}, χ_{c1} and χ_{c2} production at $\sqrt{s} = 7$ TeV*, *JHEP* **10** (2013) 115 [arXiv:1307.4285] [INSPIRE].

[14] ATLAS collaboration, *Observation of a new χ_b state in radiative transitions to $\Upsilon(1S)$ and $\Upsilon(2S)$ at ATLAS*, *Phys. Rev. Lett.* **108** (2012) 152001 [arXiv:1112.5154] [INSPIRE].

[15] D0 collaboration, V.M. Abazov et al., *Observation of a narrow mass state decaying into $\Upsilon(1S) + \gamma$ in $p\bar{p}$ collisions at $\sqrt{s} = 1.96$ TeV*, *Phys. Rev.* **D 86** (2012) 031103 [arXiv:1203.6034] [INSPIRE].

[16] L. Motyka and K. Zalewski, *Mass spectra and leptonic decay widths of heavy quarkonia*, *Eur. Phys. J.* **C 4** (1998) 107 [hep-ph/9709254] [INSPIRE].

[17] W. Kwong and J.L. Rosner, *D wave quarkonium levels of the Υ family*, *Phys. Rev.* **D 38** (1988) 279 [INSPIRE].

[18] J. Ferretti, G. Galatà and E. Santopinto, *Quark structure of the $X(3872)$ and $\chi_b(3P)$ resonances*, arXiv:1401.4431 [INSPIRE].

[19] Particle Data Group collaboration, J. Beringer et al., *Review of particle physics (RPP)*, *Phys. Rev.* **D 86** (2012) 010001 [INSPIRE] and 2013 partial update for the 2014 edition.

[20] LHCb collaboration, *The LHCb detector at the LHC*, 2008 *JINST* **3** S08005 [INSPIRE].

[21] T. Sjöstrand, S. Mrenna and P.Z. Skands, *PYTHIA* 6.4 *physics and manual*, *JHEP* **05** (2006) 026 [hep-ph/0603175] [INSPIRE].

[22] T. Sjöstrand, S. Mrenna and P.Z. Skands, *A brief introduction to PYTHIA* 8.1, *Comput. Phys. Commun.* **178** (2008) 852 [arXiv:0710.3820] [INSPIRE].

[23] I. Belyaev et al., *Handling of the generation of primary events in Gauss, the LHCb simulation framework*, *IEEE Nucl. Sci. Symp. Conf. Rec.* (2010) 1155 [INSPIRE].

[24] D.J. Lange, *The EvtGen particle decay simulation package*, *Nucl. Instrum. Meth.* **A 462** (2001) 152 [INSPIRE].

[25] P. Golonka and Z. Was, *PHOTOS Monte Carlo: a precision tool for QED corrections in Z and W decays*, *Eur. Phys. J.* **C 45** (2006) 97 [hep-ph/0506026] [INSPIRE].

[26] Geant4 collaboration, *GEANT4 developments and applications*, *IEEE Trans. Nucl. Sci.* **53** (2006) 270 [INSPIRE].

[27] Geant4 collaboration, S. Agostinelli et al., *GEANT4: a simulation toolkit*, *Nucl. Instrum. Meth.* **A 506** (2003) 250 [INSPIRE].

[28] M. Clemencic et al., *The LHCb simulation application, Gauss: design, evolution and experience*, *J. Phys. Conf. Ser.* **331** (2011) 032023 [INSPIRE].

[29] T. Skwarnicki, *A study of the radiative CASCADE transitions between the Υ' and Υ resonances*, Ph.D. thesis, Institute of Nuclear Physics, Krakow Poland (1986) [DESY-F31-86-02] [INSPIRE].

[30] CMS collaboration, *Measurement of the production cross section ratio $\sigma(\chi_{b2}(1P))/\sigma(\chi_{b1}(1P))$ in pp collisions at $\sqrt{s} = 8$ TeV*, arXiv:1409.5761 [INSPIRE].

[31] LHCb collaboration, *Study of χ_b meson production in pp collisions at $\sqrt{s} = 7$ and 8 TeV and observation of the decay $\chi_b(3P) \to \Upsilon(3S)\gamma$*, submitted to *Eur. Phys. J.* **C** [arXiv:1407.7734] [INSPIRE].

JHEP10(2014)088

The LHCb collaboration

R. Aaij[41], B. Adeva[37], M. Adinolfi[46], A. Affolder[52], Z. Ajaltouni[5], S. Akar[6], J. Albrecht[9], F. Alessio[38], M. Alexander[51], S. Ali[41], G. Alkhazov[30], P. Alvarez Cartelle[37], A.A. Alves Jr[25,38], S. Amato[2], S. Amerio[22], Y. Amhis[7], L. An[3], L. Anderlini[17,g], J. Anderson[40], R. Andreassen[57], M. Andreotti[16,f], J.E. Andrews[58], R.B. Appleby[54], O. Aquines Gutierrez[10], F. Archilli[38], A. Artamonov[35], M. Artuso[59], E. Aslanides[6], G. Auriemma[25,n], M. Baalouch[5], S. Bachmann[11], J.J. Back[48], A. Badalov[36], C. Baesso[60], W. Baldini[16], R.J. Barlow[54], C. Barschel[38], S. Barsuk[7], W. Barter[47], V. Batozskaya[28], V. Battista[39], A. Bay[39], L. Beaucourt[4], J. Beddow[51], F. Bedeschi[23], I. Bediaga[1], S. Belogurov[31], K. Belous[35], I. Belyaev[31], E. Ben-Haim[8], G. Bencivenni[18], S. Benson[38], J. Benton[46], A. Berezhnoy[32], R. Bernet[40], M.-O. Bettler[47], M. van Beuzekom[41], A. Bien[11], S. Bifani[45], T. Bird[54], A. Bizzeti[17,i], P.M. Bjørnstad[54], T. Blake[48], F. Blanc[39], J. Blouw[10], S. Blusk[59], V. Bocci[25], A. Bondar[34], N. Bondar[30,38], W. Bonivento[15,38], S. Borghi[54], A. Borgia[59], M. Borsato[7], T.J.V. Bowcock[52], E. Bowen[40], C. Bozzi[16], T. Brambach[9], J. van den Brand[42], J. Bressieux[39], D. Brett[54], M. Britsch[10], T. Britton[59], J. Brodzicka[54], N.H. Brook[46], H. Brown[52], A. Bursche[40], G. Busetto[22,r], J. Buytaert[38], S. Cadeddu[15], R. Calabrese[16,f], M. Calvi[20,k], M. Calvo Gomez[36,p], P. Campana[18,38], D. Campora Perez[38], A. Carbone[14,d], G. Carboni[24,l], R. Cardinale[19,38,j], A. Cardini[15], L. Carson[50], K. Carvalho Akiba[2], G. Casse[52], L. Cassina[20], L. Castillo Garcia[38], M. Cattaneo[38], Ch. Cauet[9], R. Cenci[58], M. Charles[8], Ph. Charpentier[38], M. Chefdeville[4], S. Chen[54], S.-F. Cheung[55], N. Chiapolini[40], M. Chrzaszcz[40,26], K. Ciba[38], X. Cid Vidal[38], G. Ciezarek[53], P.E.L. Clarke[50], M. Clemencic[38], H.V. Cliff[47], J. Closier[38], V. Coco[38], J. Cogan[6], E. Cogneras[5], L. Cojocariu[29], P. Collins[38], A. Comerma-Montells[11], A. Contu[15], A. Cook[46], M. Coombes[46], S. Coquereau[8], G. Corti[38], M. Corvo[16,f], I. Counts[56], B. Couturier[38], G.A. Cowan[50], D.C. Craik[48], M. Cruz Torres[60], S. Cunliffe[53], R. Currie[50], C. D'Ambrosio[38], J. Dalseno[46], P. David[8], P.N.Y. David[41], A. Davis[57], K. De Bruyn[41], S. De Capua[54], M. De Cian[11], J.M. De Miranda[1], L. De Paula[2], W. De Silva[57], P. De Simone[18], D. Decamp[4], M. Deckenhoff[9], L. Del Buono[8], N. Déléage[4], D. Derkach[55], O. Deschamps[5], F. Dettori[38], A. Di Canto[38], H. Dijkstra[38], S. Donleavy[52], F. Dordei[11], M. Dorigo[39], A. Dosil Suárez[37], D. Dossett[48], A. Dovbnya[43], K. Dreimanis[52], G. Dujany[54], F. Dupertuis[39], P. Durante[38], R. Dzhelyadin[35], A. Dziurda[26], A. Dzyuba[30], S. Easo[49,38], U. Egede[53], V. Egorychev[31], S. Eidelman[34], S. Eisenhardt[50], U. Eitschberger[9], R. Ekelhof[9], L. Eklund[51], I. El Rifai[5], Ch. Elsasser[40], S. Ely[59], S. Esen[11], H.-M. Evans[47], T. Evans[55], A. Falabella[14], C. Färber[11], C. Farinelli[41], N. Farley[45], S. Farry[52], RF Fay[52], D. Ferguson[50], V. Fernandez Albor[37], F. Ferreira Rodrigues[1], M. Ferro-Luzzi[38], S. Filippov[33], M. Fiore[16,f], M. Fiorini[16,f], M. Firlej[27], C. Fitzpatrick[39], T. Fiutowski[27], M. Fontana[10], F. Fontanelli[19,j], R. Forty[38], O. Francisco[2], M. Frank[38], C. Frei[38], M. Frosini[17,38,g], J. Fu[21,38], E. Furfaro[24,l], A. Gallas Torreira[37], D. Galli[14,d], S. Gallorini[22], S. Gambetta[19,j], M. Gandelman[2], P. Gandini[59], Y. Gao[3], J. García Pardiñas[37], J. Garofoli[59], J. Garra Tico[47], L. Garrido[36], C. Gaspar[38], R. Gauld[55], L. Gavardi[9], G. Gavrilov[30], A. Geraci[21,v], E. Gersabeck[11], M. Gersabeck[54], T. Gershon[48], Ph. Ghez[4], A. Gianelle[22], S. Gianì[39], V. Gibson[47], L. Giubega[29], V.V. Gligorov[38], C. Göbel[60], D. Golubkov[31], A. Golutvin[53,31,38], A. Gomes[1,a], C. Gotti[20], M. Grabalosa Gándara[5], R. Graciani Diaz[36], L.A. Granado Cardoso[38], E. Graugés[36], G. Graziani[17], A. Grecu[29], E. Greening[55], S. Gregson[47], P. Griffith[45], L. Grillo[11], O. Grünberg[62], B. Gui[59], E. Gushchin[33], Yu. Guz[35,38], T. Gys[38], C. Hadjivasiliou[59], G. Haefeli[39], C. Haen[38], S.C. Haines[47], S. Hall[53], B. Hamilton[58], T. Hampson[46], X. Han[11], S. Hansmann-Menzemer[11], N. Harnew[55], S.T. Harnew[46], J. Harrison[54], J. He[38], T. Head[38], V. Heijne[41], K. Hennessy[52], P. Henrard[5], L. Henry[8], J.A. Hernando Morata[37], E. van Herwijnen[38], M. Heß[62], A. Hicheur[1], D. Hill[55], M. Hoballah[5], C. Hombach[54], W. Hulsbergen[41], P. Hunt[55], N. Hussain[55],

JHEP10(2014)088

D. Hutchcroft[52], D. Hynds[51], M. Idzik[27], P. Ilten[56], R. Jacobsson[38], A. Jaeger[11], J. Jalocha[55], E. Jans[41], P. Jaton[39], A. Jawahery[58], F. Jing[3], M. John[55], D. Johnson[38], C.R. Jones[47], C. Joram[38], B. Jost[38], N. Jurik[59], S. Kandybei[43], W. Kanso[6], M. Karacson[38], T.M. Karbach[38], S. Karodia[51], M. Kelsey[59], I.R. Kenyon[45], T. Ketel[42], B. Khanji[20], C. Khurewathanakul[39], S. Klaver[54], K. Klimaszewski[28], O. Kochebina[7], M. Kolpin[11], I. Komarov[39], R.F. Koopman[42], P. Koppenburg[41,38], M. Korolev[32], A. Kozlinskiy[41], L. Kravchuk[33], K. Kreplin[11], M. Kreps[48], G. Krocker[11], P. Krokovny[34], F. Kruse[9], W. Kucewicz[26,o], M. Kucharczyk[20,26,38,k], V. Kudryavtsev[34], K. Kurek[28], T. Kvaratskheliya[31], V.N. La Thi[39], D. Lacarrere[38], G. Lafferty[54], A. Lai[15], D. Lambert[50], R.W. Lambert[42], G. Lanfranchi[18], C. Langenbruch[48], B. Langhans[38], T. Latham[48], C. Lazzeroni[45], R. Le Gac[6], J. van Leerdam[41], J.-P. Lees[4], R. Lefèvre[5], A. Leflat[32], J. Lefrançois[7], S. Leo[23], O. Leroy[6], T. Lesiak[26], M. Lespinasse[4], B. Leverington[11], Y. Li[3], T. Likhomanenko[63], M. Liles[52], R. Lindner[38], C. Linn[38], F. Lionetto[40], B. Liu[15], S. Lohn[38], I. Longstaff[51], J.H. Lopes[2], N. Lopez-March[39], P. Lowdon[40], H. Lu[3], D. Lucchesi[22,r], H. Luo[50], A. Lupato[22], E. Luppi[16,f], O. Lupton[55], F. Machefert[7], I.V. Machikhiliyan[31], F. Maciuc[29], O. Maev[30], S. Malde[55], A. Malinin[63], G. Manca[15,e], G. Mancinelli[6], A. Mapelli[38], J. Maratas[5], J.F. Marchand[4], U. Marconi[14], C. Marin Benito[36], P. Marino[23,t], R. Märki[39], J. Marks[11], G. Martellotti[25], A. Martens[8], A. Martín Sánchez[7], M. Martinelli[39], D. Martinez Santos[42], F. Martinez Vidal[64], D. Martins Tostes[2], A. Massafferri[1], R. Matev[38], Z. Mathe[38], C. Matteuzzi[20], A. Mazurov[16,f], M. McCann[53], J. McCarthy[45], A. McNab[54], R. McNulty[12], B. McSkelly[52], B. Meadows[57], F. Meier[9], M. Meissner[11], M. Merk[41], D.A. Milanes[8], M.-N. Minard[4], N. Moggi[14], J. Molina Rodriguez[60], S. Monteil[5], M. Morandin[22], P. Morawski[27], A. Mordà[6], M.J. Morello[23,t], J. Moron[27], A.-B. Morris[50], R. Mountain[59], F. Muheim[50], K. Müller[40], M. Mussini[14], B. Muster[39], P. Naik[46], T. Nakada[39], R. Nandakumar[49], I. Nasteva[2], M. Needham[50], N. Neri[21], S. Neubert[38], N. Neufeld[38], M. Neuner[11], A.D. Nguyen[39], T.D. Nguyen[39], C. Nguyen-Mau[39,q], M. Nicol[7], V. Niess[5], R. Niet[9], N. Nikitin[32], T. Nikodem[11], A. Novoselov[35], D.P. O'Hanlon[48], A. Oblakowska-Mucha[27], V. Obraztsov[35], S. Oggero[41], S. Ogilvy[51], O. Okhrimenko[44], R. Oldeman[15,e], C.J.G. Onderwater[65], M. Orlandea[29], J.M. Otalora Goicochea[2], P. Owen[53], A. Oyanguren[64], B.K. Pal[59], A. Palano[13,c], F. Palombo[21,u], M. Palutan[18], J. Panman[38], A. Papanestis[49,38], M. Pappagallo[51], L.L. Pappalardo[16,f], C. Parkes[54], C.J. Parkinson[9,45], G. Passaleva[17], G.D. Patel[52], M. Patel[53], C. Patrignani[19,j], A. Pearce[54], A. Pellegrino[41], M. Pepe Altarelli[38], S. Perazzini[14,d], P. Perret[5], M. Perrin-Terrin[6], L. Pescatore[45], E. Pesen[66], K. Petridis[53], A. Petrolini[19,j], E. Picatoste Olloqui[36], B. Pietrzyk[4], T. Pilař[48], D. Pinci[25], A. Pistone[19], S. Playfer[50], M. Plo Casasus[37], F. Polci[8], A. Poluektov[48,34], E. Polycarpo[2], A. Popov[35], D. Popov[10], B. Popovici[29], C. Potterat[2], E. Price[46], J. Prisciandaro[39], A. Pritchard[52], C. Prouve[46], V. Pugatch[44], A. Puig Navarro[39], G. Punzi[23,s], W. Qian[4], B. Rachwal[26], J.H. Rademacker[46], B. Rakotomiaramanana[39], M. Rama[18], M.S. Rangel[2], I. Raniuk[43], N. Rauschmayr[38], G. Raven[42], S. Reichert[54], M.M. Reid[48], A.C. dos Reis[1], S. Ricciardi[49], S. Richards[46], M. Rihl[38], K. Rinnert[52], V. Rives Molina[36], D.A. Roa Romero[5], P. Robbe[7], A.B. Rodrigues[1], E. Rodrigues[54], P. Rodriguez Perez[54], S. Roiser[38], V. Romanovsky[35], A. Romero Vidal[37], M. Rotondo[22], J. Rouvinet[39], T. Ruf[38], H. Ruiz[36], P. Ruiz Valls[64], J.J. Saborido Silva[37], N. Sagidova[30], P. Sail[51], B. Saitta[15,e], V. Salustino Guimaraes[2], C. Sanchez Mayordomo[64], B. Sanmartin Sedes[37], R. Santacesaria[25], C. Santamarina Rios[37], E. Santovetti[24,l], A. Sarti[18,m], C. Satriano[25,n], A. Satta[24], D.M. Saunders[46], D. Savrina[31,32], M. Schiller[42], H. Schindler[38], M. Schlupp[9], M. Schmelling[10], B. Schmidt[38], O. Schneider[39], A. Schopper[38], M.-H. Schune[7], R. Schwemmer[38], B. Sciascia[18], A. Sciubba[25], A. Semennikov[31], I. Sepp[53], N. Serra[40], J. Serrano[6], L. Sestini[22], P. Seyfert[11], M. Shapkin[35], I. Shapoval[16,43,f], Y. Shcheglov[30], T. Shears[52], L. Shekhtman[34], V. Shevchenko[63], A. Shires[9], R. Silva Coutinho[48], G. Simi[22], M. Sirendi[47], N. Skidmore[46], T. Skwarnicki[59], N.A. Smith[52], E. Smith[55,49], E. Smith[53],

JHEP10(2014)088

J. Smith[47], M. Smith[54], H. Snoek[41], M.D. Sokoloff[57], F.J.P. Soler[51], F. Soomro[39], D. Souza[46], B. Souza De Paula[2], B. Spaan[9], A. Sparkes[50], P. Spradlin[51], S. Sridharan[38], F. Stagni[38], M. Stahl[11], S. Stahl[11], O. Steinkamp[40], O. Stenyakin[35], S. Stevenson[55], S. Stoica[29], S. Stone[59], B. Storaci[40], S. Stracka[23,38], M. Straticiuc[29], U. Straumann[40], R. Stroili[22], V.K. Subbiah[38], L. Sun[57], W. Sutcliffe[53], K. Swientek[27], S. Swientek[9], V. Syropoulos[42], M. Szczekowski[28], P. Szczypka[39,38], T. Szumlak[27], S. T'Jampens[4], M. Teklishyn[7], G. Tellarini[16,f], F. Teubert[38], C. Thomas[55], E. Thomas[38], J. van Tilburg[41], V. Tisserand[4], M. Tobin[39], S. Tolk[42], L. Tomassetti[16,f], D. Tonelli[38], S. Topp-Joergensen[55], N. Torr[55], E. Tournefier[4], S. Tourneur[39], M.T. Tran[39], M. Tresch[40], A. Trisovic[38], A. Tsaregorodtsev[6], P. Tsopelas[41], N. Tuning[41], M. Ubeda Garcia[38], A. Ukleja[28], A. Ustyuzhanin[63], U. Uwer[11], V. Vagnoni[14], G. Valenti[14], A. Vallier[7], R. Vazquez Gomez[18], P. Vazquez Regueiro[37], C. Vázquez Sierra[37], S. Vecchi[16], J.J. Velthuis[46], M. Veltri[17,h], G. Veneziano[39], M. Vesterinen[11], B. Viaud[7], D. Vieira[2], M. Vieites Diaz[37], X. Vilasis-Cardona[36,p], A. Vollhardt[40], D. Volyanskyy[10], D. Voong[46], A. Vorobyev[30], V. Vorobyev[34], C. Voß[62], J.A. de Vries[41], R. Waldi[62], C. Wallace[48], R. Wallace[12], J. Walsh[23], S. Wandernoth[11], J. Wang[59], D.R. Ward[47], N.K. Watson[45], D. Websdale[53], M. Whitehead[48], J. Wicht[38], D. Wiedner[11], G. Wilkinson[55], M.P. Williams[45], M. Williams[56], F.F. Wilson[49], J. Wimberley[58], J. Wishahi[9], W. Wislicki[28], M. Witek[26], G. Wormser[7], S.A. Wotton[47], S. Wright[47], S. Wu[3], K. Wyllie[38], Y. Xie[61], Z. Xing[59], Z. Xu[39], Z. Yang[3], X. Yuan[3], O. Yushchenko[35], M. Zangoli[14], M. Zavertyaev[10,b], L. Zhang[59], W.C. Zhang[12], Y. Zhang[3], A. Zhelezov[11], A. Zhokhov[31], L. Zhong[3] and A. Zvyagin[38].

[1] *Centro Brasileiro de Pesquisas Físicas (CBPF), Rio de Janeiro, Brazil*
[2] *Universidade Federal do Rio de Janeiro (UFRJ), Rio de Janeiro, Brazil*
[3] *Center for High Energy Physics, Tsinghua University, Beijing, China*
[4] *LAPP, Université de Savoie, CNRS/IN2P3, Annecy-Le-Vieux, France*
[5] *Clermont Université, Université Blaise Pascal, CNRS/IN2P3, LPC, Clermont-Ferrand, France*
[6] *CPPM, Aix-Marseille Université, CNRS/IN2P3, Marseille, France*
[7] *LAL, Université Paris-Sud, CNRS/IN2P3, Orsay, France*
[8] *LPNHE, Université Pierre et Marie Curie, Université Paris Diderot, CNRS/IN2P3, Paris, France*
[9] *Fakultät Physik, Technische Universität Dortmund, Dortmund, Germany*
[10] *Max-Planck-Institut für Kernphysik (MPIK), Heidelberg, Germany*
[11] *Physikalisches Institut, Ruprecht-Karls-Universität Heidelberg, Heidelberg, Germany*
[12] *School of Physics, University College Dublin, Dublin, Ireland*
[13] *Sezione INFN di Bari, Bari, Italy*
[14] *Sezione INFN di Bologna, Bologna, Italy*
[15] *Sezione INFN di Cagliari, Cagliari, Italy*
[16] *Sezione INFN di Ferrara, Ferrara, Italy*
[17] *Sezione INFN di Firenze, Firenze, Italy*
[18] *Laboratori Nazionali dell'INFN di Frascati, Frascati, Italy*
[19] *Sezione INFN di Genova, Genova, Italy*
[20] *Sezione INFN di Milano Bicocca, Milano, Italy*
[21] *Sezione INFN di Milano, Milano, Italy*
[22] *Sezione INFN di Padova, Padova, Italy*
[23] *Sezione INFN di Pisa, Pisa, Italy*
[24] *Sezione INFN di Roma Tor Vergata, Roma, Italy*
[25] *Sezione INFN di Roma La Sapienza, Roma, Italy*
[26] *Henryk Niewodniczanski Institute of Nuclear Physics Polish Academy of Sciences, Kraków, Poland*
[27] *AGH - University of Science and Technology, Faculty of Physics and Applied Computer Science, Kraków, Poland*
[28] *National Center for Nuclear Research (NCBJ), Warsaw, Poland*

JHEP10(2014)088

[29] Horia Hulubei National Institute of Physics and Nuclear Engineering, Bucharest-Magurele, Romania
[30] Petersburg Nuclear Physics Institute (PNPI), Gatchina, Russia
[31] Institute of Theoretical and Experimental Physics (ITEP), Moscow, Russia
[32] Institute of Nuclear Physics, Moscow State University (SINP MSU), Moscow, Russia
[33] Institute for Nuclear Research of the Russian Academy of Sciences (INR RAN), Moscow, Russia
[34] Budker Institute of Nuclear Physics (SB RAS) and Novosibirsk State University, Novosibirsk, Russia
[35] Institute for High Energy Physics (IHEP), Protvino, Russia
[36] Universitat de Barcelona, Barcelona, Spain
[37] Universidad de Santiago de Compostela, Santiago de Compostela, Spain
[38] European Organization for Nuclear Research (CERN), Geneva, Switzerland
[39] Ecole Polytechnique Fédérale de Lausanne (EPFL), Lausanne, Switzerland
[40] Physik-Institut, Universität Zürich, Zürich, Switzerland
[41] Nikhef National Institute for Subatomic Physics, Amsterdam, The Netherlands
[42] Nikhef National Institute for Subatomic Physics and VU University Amsterdam, Amsterdam, The Netherlands
[43] NSC Kharkiv Institute of Physics and Technology (NSC KIPT), Kharkiv, Ukraine
[44] Institute for Nuclear Research of the National Academy of Sciences (KINR), Kyiv, Ukraine
[45] University of Birmingham, Birmingham, United Kingdom
[46] H.H. Wills Physics Laboratory, University of Bristol, Bristol, United Kingdom
[47] Cavendish Laboratory, University of Cambridge, Cambridge, United Kingdom
[48] Department of Physics, University of Warwick, Coventry, United Kingdom
[49] STFC Rutherford Appleton Laboratory, Didcot, United Kingdom
[50] School of Physics and Astronomy, University of Edinburgh, Edinburgh, United Kingdom
[51] School of Physics and Astronomy, University of Glasgow, Glasgow, United Kingdom
[52] Oliver Lodge Laboratory, University of Liverpool, Liverpool, United Kingdom
[53] Imperial College London, London, United Kingdom
[54] School of Physics and Astronomy, University of Manchester, Manchester, United Kingdom
[55] Department of Physics, University of Oxford, Oxford, United Kingdom
[56] Massachusetts Institute of Technology, Cambridge, MA, United States
[57] University of Cincinnati, Cincinnati, OH, United States
[58] University of Maryland, College Park, MD, United States
[59] Syracuse University, Syracuse, NY, United States
[60] Pontifícia Universidade Católica do Rio de Janeiro (PUC-Rio), Rio de Janeiro, Brazil, associated to [2]
[61] Institute of Particle Physics, Central China Normal University, Wuhan, Hubei, China, associated to [3]
[62] Institut für Physik, Universität Rostock, Rostock, Germany, associated to [11]
[63] National Research Centre Kurchatov Institute, Moscow, Russia, associated to [31]
[64] Instituto de Fisica Corpuscular (IFIC), Universitat de Valencia-CSIC, Valencia, Spain, associated to [36]
[65] Van Swinderen Institute, University of Groningen, Groningen, The Netherlands, associated to [41]
[66] Celal Bayar University, Manisa, Turkey, associated to [38]
[a] Universidade Federal do Triângulo Mineiro (UFTM), Uberaba-MG, Brazil
[b] P.N. Lebedev Physical Institute, Russian Academy of Science (LPI RAS), Moscow, Russia
[c] Università di Bari, Bari, Italy
[d] Università di Bologna, Bologna, Italy
[e] Università di Cagliari, Cagliari, Italy
[f] Università di Ferrara, Ferrara, Italy
[g] Università di Firenze, Firenze, Italy
[h] Università di Urbino, Urbino, Italy

JHEP10(2014)088

[i] *Università di Modena e Reggio Emilia, Modena, Italy*
[j] *Università di Genova, Genova, Italy*
[k] *Università di Milano Bicocca, Milano, Italy*
[l] *Università di Roma Tor Vergata, Roma, Italy*
[m] *Università di Roma La Sapienza, Roma, Italy*
[n] *Università della Basilicata, Potenza, Italy*
[o] *AGH - University of Science and Technology, Faculty of Computer Science, Electronics and Telecommunications, Kraków, Poland*
[p] *LIFAELS, La Salle, Universitat Ramon Llull, Barcelona, Spain*
[q] *Hanoi University of Science, Hanoi, Viet Nam*
[r] *Università di Padova, Padova, Italy*
[s] *Università di Pisa, Pisa, Italy*
[t] *Scuola Normale Superiore, Pisa, Italy*
[u] *Università degli Studi di Milano, Milano, Italy*
[v] *Politecnico di Milano, Milano, Italy*

JHEP10(2014)088